Supplementary Information for:

Molecular determinants of chaperone interactions on MHC-I for folding and antigen repertoire selection

Andrew C. McShan[1†], Christine A. Devlin[2†], Sarah A. Overall[1], Jihye Park[2], Jugmohit S. Toor[1], Danai Moschidi[1], David Flores-Solis[1, ‡], Hannah Choi[2], Sarvind Tripathi[1], Erik Procko[2*] and Nikolaos G. Sgourakis[1*]

[1]Department of Chemistry and Biochemistry, University of California Santa Cruz, Santa Cruz, CA 95064, USA.

[2]Department of Biochemistry and Cancer Center at Illinois, University of Illinois, Urbana, IL 61801, USA.

‡ Current address: Max Planck Institute for Biophysical Chemistry Am Fassberg 11 37077 Göttingen, Germany

† These authors contributed equally to this work.

* To whom correspondence should be addressed: Erik Procko (procko@illinois.edu) or Nikolaos G. Sgourakis (nsgourak@ucsc.edu).

This PDF file includes:

Supplemental Methods

Expression Constructs for Cell Assays. Expi293F cells (ThermoFisher) were cultured in Expi293 Expression Medium (ThermoFisher) at 37 °C, 125 rpm, and 8% CO_2. FLAG-TAPBPR (containing from N- to C-terminus the signal peptide of influenza HA, a FLAG tag, a GGS linker, and TAPBPR residues K1-S447) was PCR assembled. TAPBPR-TM was assembled by fusing the ectodomain of FLAG-TAPBPR up to residue R384, followed by a SGAGSA linker, on to amino acids (a.a.) I282-D314 of HLA-G encoding a canonical transmembrane domain. Tagged MHC-I alleles were constructed featuring from N- to C-terminus the signal peptide of influenza HA, a c-myc tag, a GSPGGSSGGG linker, and mature MHC-I. H2-D_d constructs carried the C121S mutation, removing a non-oxidized extracellular cysteine residue to prevent spurious disulfide formation during engineering. For BiFC experiments, the C-termini of FLAG-TAPBPR and FLAG-TAPBPR-TM were fused to VC (a.a. D155–K238 of Venus). The C-termini of myc-tagged MHC-I were fused to VN (a.a. V1–A154 of Venus I152L mutant) (*1*). Cloning of tagged CXCR4 fusions to VN and VC are previously described (*2*). All constructs were cloned into pCEP4 (Invitrogen), and targeted mutations were generated by site directed mutagenesis and confirmed with DNA sequencing. Plasmids will be available from Addgene upon publication.

Bimolecular Fluorescence Complementation. Expi293F cells at 2×10^6 per mL were co-transfected with 500 ng of plasmids encoding the respective VN- and VC-fusions using ExpiFectamine (ThermoFisher). Cells were harvested 23-25 h post transfection and fixed using BD Fixation/Permeabilization kit (BD Biosciences). Cells were washed with BD Perm/Wash Buffer, stained with anti-FLAG Cy3 (clone M2, 1/200 dilution; Sigma-Aldrich) and anti-myc Alexa 647 (clone 9B11, 1/200 dilution; Cell Signaling Technology), washed twice, and resuspended in Dulbecco's phosphate-buffered saline (PBS) supplemented with 0.2% bovine serum albumin (BSA) for analysis on a BD LSR II with three-color compensation. Data were analyzed with FCS Express 6 (De Novo Software).

Immunoblots. Cell samples were denatured in reducing sodium dodecyl sulfate (SDS) load dye, and proteins were separated by gel electrophoresis and transferred to polyvinylidene difluoride membrane. For FLAG-tagged proteins, membranes were blocked with 3% BSA in Tris-buffered saline-0.1% Tween 20 (TBST), incubated in 1/2,000 anti-FLAG (M2) AP (Sigma-Aldrich), washed thoroughly and detected with 1-Step NBT-BCIP (ThermoFisher). Blots for myc-tagged proteins were blocked with 5% BSA in TBST, incubated in 1/2,000 anti-myc (71D10) HRP (Cell Signaling Technology), and detected using Clarity Western ECL substrate (Bio-Rad).

Immunoprecipitations. Transfected Expi293F cells were harvested 23-25 h post transfection and freeze-thawed twice in PBS supplemented with protease inhibitors (Sigma-Aldrich). Lysed samples were centrifuged at 21,000 g. Membrane pellets were solubilized with precipitation buffer (50 mM Tris pH 7.5, 150 mM NaCl, 5 mM $MgCl_2$, 1 mM EDTA) containing 0.5% dodecylmaltoside (DDM; Anatrace). Insoluble debris was removed by centrifugation at 21,000 g. The soluble fraction was incubated with FLAG M2 resin (Sigma-Aldrich) for 1 h at 4 °C, and then washed three times with precipitation buffer containing 0.05% DDM. Resin was resuspended in reducing SDS load dye for immunoblotting.

Library Generation. Using the pCEP4-myc-HLA-A*02:01-VN expression plasmid, a SSM library focused on the α_1/α_2 domains (a.a. S2-R181) was created using overlap extension PCR (*3*). The library covered 3,524 of 3,600 possible single amino acid substitutions based on a minimum frequency of 2×10^{-6}. Expi293F cells at 2×10^6 cells/mL were transfected using Expifectamine (ThermoFisher) with 1 ng library DNA diluted with 1.5 μg of pCEP4-ΔCMV (*4*). The media was replaced 2 hours post transfection. Under these conditions, cells typically acquire no more than a single coding sequence (*2*).

Sorting for Myc-HLA-A*02:01 Surface Expression. Expi293F cells were harvested 25 h post-transfection. Cells were washed on ice with PBS-BSA, stained with Alexa Fluor 647-conjugated anti-myc clone 9B11 (1:200 dilution; Cell Signaling Technology), washed twice and resuspended in PBS-BSA. Cells were stained with propidium iodide (final concentration of 1 μg/mL) immediately prior to sorting. Cells were gated by scattering properties to exclude debris and doublets, and propidium iodide-positive cells were also excluded. The top 0.5% of cells for Alexa Fluor 647 fluorescence were collected into fetal bovine serum coated tubes containing media during a 4 h sort on a BD FACSAria II. Collected cells were pelleted and frozen at -80 °C. Replicate selections were performed independently on different days.

Sorting for BiFC Signal. Expi293F cells were transfected with pCEP4-FLAG-TAPBPR-TM-VC linearized by EcoRV, selected with 100 μg/ml hygromycin B, and FACS sorted for FLAG positive cells. The resulting stable line was transfected with the library as described above. Cells were harvested 25 h post-transfection, washed and resuspended in ice-cold PBS-BSA. Cells were sorted using a BD FACSAria II, excluding debris and doublets based on scattering properties. The top 20% of Venus-positive cells (equivalent to the top 1% of the total population) were collected and frozen at -80 °C.

Deep Sequencing. RNA was extracted from sorted cells using the GeneJet RNA purification kit (Fisher). cDNA was prepared using Accuscript reverse transcriptase (Agilent) with a primer that annealed to the VN region to prevent amplification of endogenous HLA-A*02:01 transcripts. DNA fragments spanning the mutated region were PCR amplified in two rounds: the first appended sequences complementary to Illumina sequencing primers, and the second added experiment-specific barcodes and Illumina adaptamers. Sequencing was on a NovaSeq 6000 and analyzed with Enrich (*5*). Data deposited with NCBI's Gene Expression Omnibus under series accession number GSE128957 includes primer sequences and commands.

Confocal Microscopy. Modified from the protocol described in (*4*). Briefly, transfected HEK293T cells were stained with one drop of NucBlue™ Live ReadyProbes™ Reagent (Thermo) per 300 ul cells for 20 min at room temperature. Cells were fixed and permeabilized using the BD Cytofix/Cytoperm kit, and stained with anti-FLAG-FITC (ICL, Inc). Images were collected on a Zeiss LSM 700 (Carl Zeiss) and processed using Fiji.

Expression Constructs for Protein Purification. DNA encoding the luminal domain of MHC-I heavy chains of murine H2-D^d and H2-L^d, and human HLA-A*02:01 and HLA-A*01:01, were transformed into *Escherichia coli* BL21(*DE3)* (Novagen). MHC-I molecules were expressed in Luria-Broth, extracted from inclusion bodies, refolded *in vitro* at 4°C and pMHC-I complexes were purified as previously described (*6*). Known full-length peptide antigens used for refolding

were prepared by chemical synthesis (Biopeptek Inc, Malvern, USA or GenScript, Piscataway, USA): NIH peptide (YPNVNIHNF) for H2-L^d (*7*); P18-I10 peptide (RGPGRAFVTI) for H2-D^d (*8*); $NRAS_{Q61K}$ peptide (ILDTAGKEEY) for HLA-A*01:01 (*9*); TAX peptide (LLFGYPVYV) for HLA-A*02:01 (*10*). The luminal domain of TAPBPR was expressed using a Drosophila S2 cell expression system and purified as previously described (*11*). All purified proteins were exhaustively buffer exchanged into 100 mM NaCl, 20 mM sodium phosphate pH 7.2.

X-ray crystallography. P18-I10/H2-$D^{d\ Y84C\text{-}A139C}$/hβ2m crystals were grown by the sitting drop method and plates were incubated at 22°C. Crystals were obtained by mixing 1 µL of protein at 12 mg/mL with an equal volume of reservoir solution (0.2M ammonium acetate, 0.1M Bis-Tris pH 5.5 and 25% (v/v) PEG 3350). Reservoir solution supplemented with 20% (v/v) glycerol used as a cryoprotectant. Data were collected at the Advanced Photon Source, Argonne National Laboratory, at beamline 23-IDB. Diffraction images were indexed, integrated, and scaled using Mosflm and Aimless in the CCP4 package (*12*). Structures were determined by Phaser (*13*) using PDB ID 3ECB as a search model. Model building and refinement were performed using COOT (*14*) and Phenix (*15*), respectively. The structural model and structure factors were deposited into the Protein Data Bank under accession code 6NPR.

Differential Scanning Fluorimetry. DSF experiments were performed on an Applied Biosystems ViiA 7 qPCR machine with excitation and emission wavelengths set to 470 nm and 569 nm with proteins in buffer of 100 mM NaCl, 20 mM sodium phosphate pH 7.2. Experiments were conducted in triplicate in MicroAmp Fast 96-well plates with 50 µL total volume containing final concentrations of 7 µM protein and 10× SYPRO orange dye (ThermoFisher). Temperature was incrementally increased at a scan rate of 1°C/min between 25°C and 95°C. Data analysis and fitting were performed in GraphPad Prism v7.

SEC Binding Assays. Size exclusion chromatography (SEC) binding assays were performed using a mixture of 80 µM pMHC-I and 80 µM TAPBPR (1:1 molar ratio) that were incubated at room temperature for 1 hour. SEC binding was performed on a Superdex 200 Increase 10/300 GL column at flow rate 0.5 mL/min in 100 mM NaCl, 20 mM sodium phosphate pH 7.2.

ITC experiments. Isothermal titration calorimetry (ITC) experiments between pMHC-I and TAPBPR constructs were obtained using a MicroCal VP-ITC system (Malvern Panalytical). All proteins were exhaustively dialyzed into the buffer (50 mM NaCl, 20 mM sodium phosphate pH 7.2) filtered through a 0.22 µm PES membrane. Syringe containing pMHC-I at concentrations of 100 to 150 µM were titrated into calorimetry cell containing 12 µM TAPBPR and 1 mM purified free peptide ($NRAS_{Q61K}$ for HLA-A*01:01, TAX for HLA-A*02:01, P18-I10 for H2-D^d and p29 for H2-L^d). Injection volumes were 10 µL performed for a duration of 10 sec and spaced 220 sec apart to allow for a complete return to baseline. Data was subtracted from a control performed where syringe containing pMHC-I at concentrations of 100 to 150 µM were titrated into calorimetry cell containing buffer and 1 mM purified free peptide. Data were processed and analyzed with Origin software. Isotherms were fit using a one-site ITC binding model. The first data point was excluded from analysis. Reported K_D, $-T*\Delta S$, and ΔH values are the average values from two technical replicates.

NMR Chemical Shift Assignments. Samples for NMR were prepared using AILV methyl (Ala $^{13}C\beta$, Ile $^{13}C\delta1$, Leu $^{13}C\delta1/^{13}C\delta2$, Val $^{13}C\gamma1/^{13}C\gamma2$) labeling at the heavy chain of H2-D^d, H2-L^d, HLA-A*02:01 or HLA-A*01:01 pMHC-I molecules, on a $^{12}C/^{2}H/^{15}N$ background (*6*). Resonance assignments were derived separately for each pMHC-I system from a series of 3D experiments recorded at 800 MHz and 25ºC (*6, 16*). Briefly, backbone amide resonances were assigned using standard, TROSY-based 3D HNCO, HNCA and HN(CA)CB experiments recorded at 800 MHz at 25ºC. Backbone amide assignments were further validated through amide-amide NOEs, acquired in 3D H^N-NH^N and 3D N-NH^N SOFAST NOESY experiments (3). Unambiguous assignments of methyl resonances were obtained on the basis of the backbone assignments, using 3D HMCM[CG]CBCA out-and-back methyl-TROSY experiments recorded on 500 µM to 1 mM pMHC-I samples prepared with an alternative ILV methyl labelling scheme (ILV*) which aims to generate a linear ^{13}C labelling pattern at the side chains of Leu and Val spin systems for optimal sensitivity (*18*). AILV methyl assignments were validated and stereo-specifically disambiguated by acquiring methyl-methyl NOEs in 3D H^M-C^MH^M and 3D C^M-C^MH^M SOFAST NOESY experiments (*17*). All 3D SOFAST NOESY experiments were acquired using standard parameters (*16*). To confirm the assignment of the TAPBPR bound pMHC-I states for the sidechain methyl resonances, an additional 3D H^M-C^MH^M experiment was acquired with 200 µM pMHC-I/TAPBPR complexes and compared to similar NOE strips from the unbound pMHC-I reference. All NMR data were processed with NMRPipe (4) and analyzed using NMRFAM-SPARKY (5).

NMR Titrations and Chemical Shift Mapping. NMR chemical shift mapping of different pMHC-I/TAPBPR complexes was performed in a manner analogous to our established characterization of the H2-D^d system (*6*). Briefly, 105 µM pMHC-I was titrated with increasing concentrations of unlabeled TAPBPR in matched NMR buffer (100 mM NaCl, 20 mM sodium phosphate pH 7.2, 10% D_2O (v/v), 1U Roche protease inhibitor). pMHC-I:TAPBPR molar ratios were 1:0, 1:0.59, 1:1.18, 1:1.77, 1:2.36, and 1:2.95. Two-dimensional ^{1}H-^{13}C methyl SOFAST HMQC experiments recorded at 25ºC at a ^{1}H field strength of 800 MHz were used as readouts. A total number of 136 scans were used with a 0.2 sec recycle delay (d1) and acquisition times of 30 ms in the ^{13}C dimension. To compare with the SOFAST experiments, an additional titration between 105 µM pMHC-I with pMHC-I:TAPBPR molar ratios were 1:0, 1:0.59, 1:1.18, 1:1.77, 1:2.36, and 1:2.95 was performed using standard (non-SOFAST) version of the 2D ^{1}H-^{13}C HMQC experiment recorded at 25ºC at a ^{1}H field strength of 800 MHz with 28 scans were used with a 0.8 sec recycle delay (d1) and acquisition times of 30 ms in the ^{13}C dimension. Data were processed with 4 Hz and 10 Hz Lorentzian line broadening in the direct and indirect dimensions, respectively, and fit using a two-state binding model in TITAN (*21*) with bootstrap error analysis of 100 replicas. Chemical shift deviations (CSD, p.p.m.) were determined using the equation $\Delta\delta_{CH3}=[1/2(\Delta\delta_{H2}+\Delta\delta_{C2}/4)]_{1/2}$ for ^{13}C AILV methyls. The $|\Delta\delta\ ^{13}C|$ was determined by taking the absolute value of the difference between the ^{13}C chemical shift of the free and TAPBPR bound pMHC-I states.

CPMG Relaxation Dispersion. AILV methyl sidechain relaxation dispersion profiles were obtained using ^{1}H to ^{13}C single-quantum Carr-Purcell-Meiboom-Gill (CPMG) relaxation dispersion experiments (*22*) on samples with concentrations ranging from 500 µM to 1 mM perdeuterated pMHC-I samples recorded at 25ºC at 600 MHz and 800 MHz. A temperature calibration using the temperature-dependence of the water resonance, relative to an internal 4,4-

demethyl-4-silapentane-1-sulfonic acid (DSS) standard was used to ensure strict temperature matching between the two instruments operating at different magnetic fields. Spectra were recorded in an interleaved manner with CPMG field strengths of 50, 100, 150, 200, 250, 300, 350, 400, 450, 500, 550, 600, 650, 700, 800, 900 and 1000 Hz with a constant time delay (T_{CPMG}) of 40 ms. Peak intensities obtained using NMRFAM-SPARKY were converted to the $R_{2,\,eff}$ transverse decay rates with the equation $R_{2,\,eff} = 1/T_{CPMG} \times \ln (I_0 / I_{vCPMG})$. Only with non-overlapping resonances were analyzed. CPMG profiles were fitted with a two-state, global model of all methyl groups displaying dispersion ($R_{ex} > 1\ s^{-1}$) using the program CATIA, which further allows for a correction of off-resonance effects of the CPMG 180° pulse train (http://www.biochem.ucl.ac.uk/hansen/catia/).

Fluorescence Anisotropy. Fluorescence anisotropy (r, herein referred to as FA) was performed using a P18-I10 peptide labeled with TAMRA dye (K_{TAMRA}GPGRAFVTI, herein called TAMRA-P18-I10) (Biopeptek Inc.) (*6*). Graded concentrations (0 μM, 0.05 μM, 0.1 μM, 0.25 μM, 0.5 μM and 1 μM) of TAPBPR were added to a mixture of 0.75 nM TAMRA-P18-I10 and either 0.1 μM of wild-type P18-I10/H2-D_d/hβ2m or P18-I10/H2-$D_{d\ Y84C-A139C}$/hβ2m. The average FA after incubation for 95–105 min at room temperature (25 °C) was plotted as a function of the $\log_{10}$ of concentration of TAPBPR. Each experiment was performed at room temperature in a volume of 100 μL and loaded onto a black 96-well polystyrene assay plate (Costar 3915). FA data were recorded via a PerkinElmer Envision 2103 plate reader with an excitation filter of λ_{ex} = 531 nm and an emission filter of λ_{em} = 595 nm. Each experiment was performed in triplicate. Experimental values were subtracted from background FA values obtained from incubation of TAMRA-P18-I10 alone. All samples were prepared in matched buffer (100 mM NaCl, 20 mM sodium phosphate pH 7.2, 0.05% (v/v) tween-20). Data analysis and fitting was performed in GraphPad Prism v7.

Rosetta modeling. *Rosetta*'s comparative modeling protocol was used to generate MHC-I/TAPBPR complexes using the H2-D_d/β2m/TAPBPR crystal structure as a template (*23*, *24*). High resolution structure refinement of the resulting models were carried out using *Rosetta*'s relax protocol (*25*).

Additional Acknowledgements. We acknowledge the Lewis Kay (University of Toronto) lab for providing the SQ ^{13}C-CPMG pulse sequences, Flemming Hansen (University College London) for aid with CPMG fitting in CATIA, Hsiau-Wei Lee (UCSC) for assistance in acquiring NMR experiments at 600 MHz, Kannan Natarajan (NIAID) for providing the S2 cell lines for TAPBPR protein expression and Tilini Wijeratne and Giora Morozov (UCSC) for help with protein expression and purification. Cell sorting and deep sequencing were conducted at the Roy J. Carver Biotechnology Center (Illinois) with assistance from Barbara Pilas, Barbara Balhan, Christy Wright, and Alvaro Hernandez. We are thankful to Kannan Natarajan and David Margulies (NIAID) for helpful discussions throughout the course of this study.

Supplemental Figures

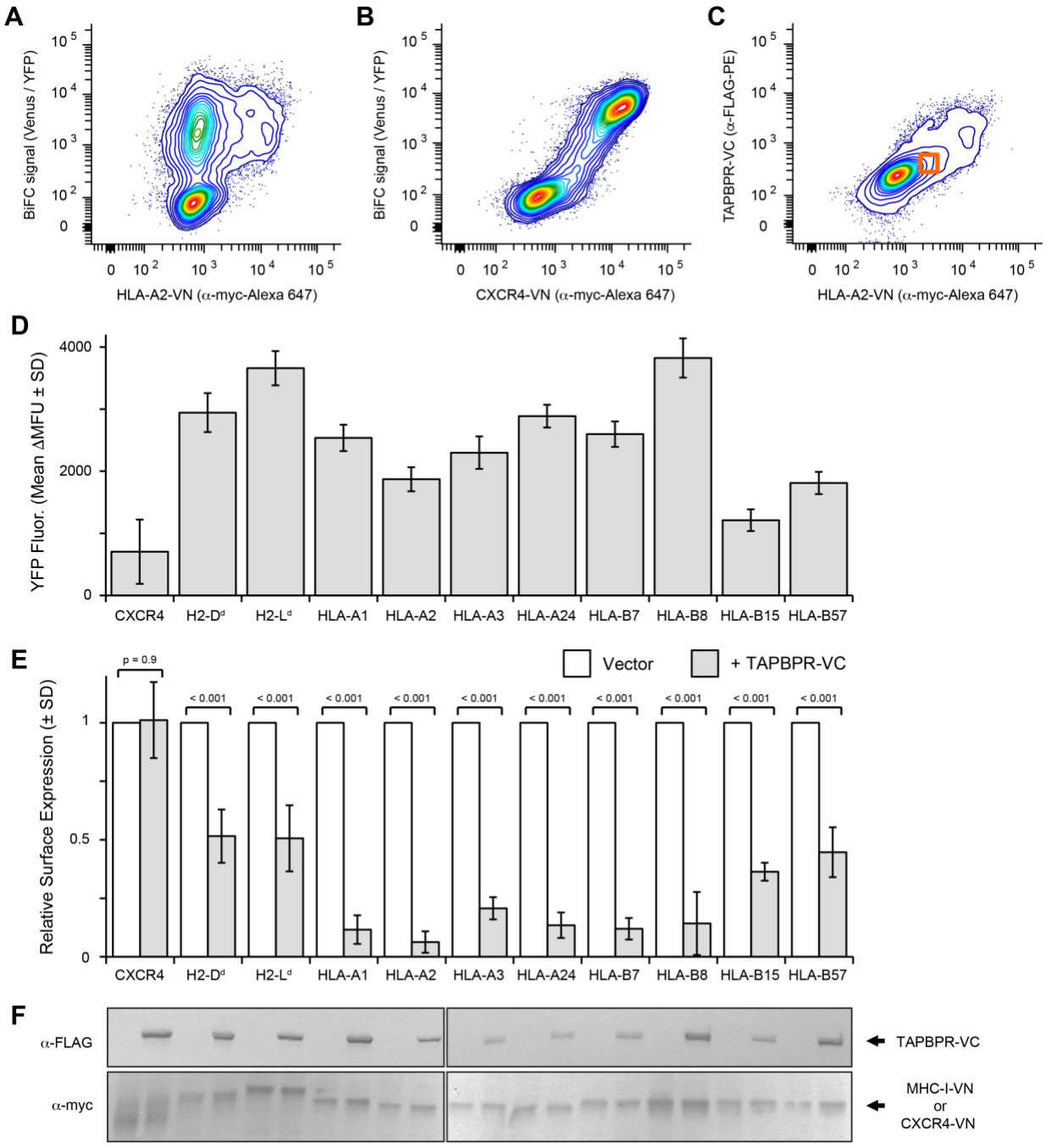

Fig. S1. TAPBPR associates with a broad range of MHC-I alleles in a native cellular environment. (A) Intracellular staining and flow cytometry analysis of Expi293F cells co-expressing myc-HLA-A*02:01-VN (*x*-axis) and FLAG-TAPBPR-VC. Venus fluorescence (*y*-axis) is high at low HLA-A*02:01 expression. **(B)** FLAG-TAPBPR-VC was co-expressed with myc-CXCR4-VN (*x*-axis) as a negative control. Venus fluorescence (*y*-axis) is only elevated at very high CXCR4 expression due to non-specific interactions. **(C)** To partially compensate for

expression differences and exclude highly expressing cells with saturated BiFC, cells were gated (orange box) for low MHC-I or CXCR4 (*x*-axis) and TAPBPR (*y*-axis) expression prior to measuring BiFC signal. **(D)** BiFC between TAPBPR-VC and CXCR4-VN or MHC-I-VN. Average ΔMean Fluorescence Units (ΔMFU) ± SD, n = 4. **(E)** Surface expression levels of myc-tagged VN constructs in the absence and presence of TAPBPR-VC were determined by flow cytometry. Mean ± SD, n = 7, *p* values determined by two-tailed Student's t test. In panels **(D)** and **(E)** the full allele names for HLA molecules tested are HLA-A*01:01, HLA-A*02:01, HLA-A*03:01, HLA-A*24:02, HLA-B*07:02, HLA-B*08:01, HLA-B*15:01 and HLA-B57:01. **(F)** Western blots for a representative experiment comparing total protein expression levels for TAPBPR (α-FLAG) and CXCR4 or heavy chain MHC-I (α-myc) constructs. Samples are vertically aligned with graphs above.

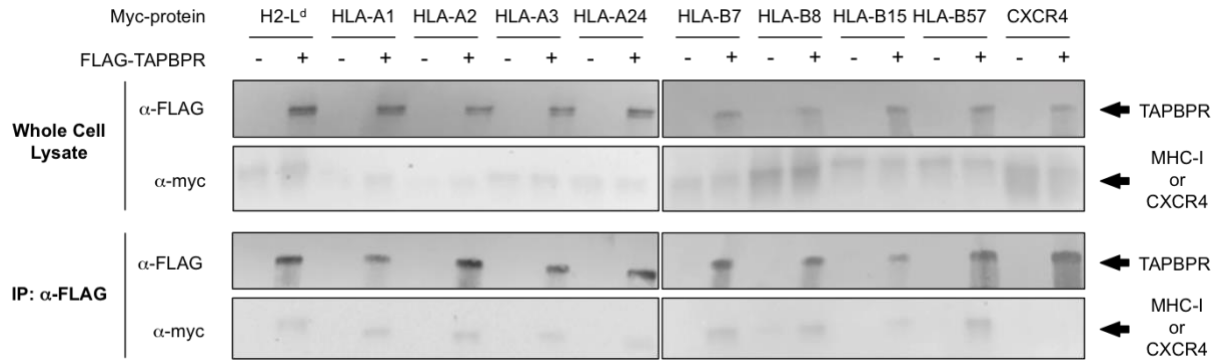

Fig. S2. TAPBPR co-immunoprecipitates with a broad range of MHC-I alleles.
FLAG-TAPBPR was co-expressed with myc-MHC-I or the negative control myc-CXCR4 (see upper immunoblots of protein in solubilized cell lysates). TAPBPR was precipitated with anti-FLAG resin and bound proteins were detected (lower immunoblots). Shown are representative results from two replicates. The full allele names for HLA molecules tested are HLA-A*01:01, HLA-A*02:01, HLA-A*03:01, HLA-A*24:02, HLA-B*07:02, HLA-B*08:01, HLA-B*15:01 and HLA-B57:01. Refer to Fig. S10 for immunoprecipitations of H2-Dd with TAPBPR.

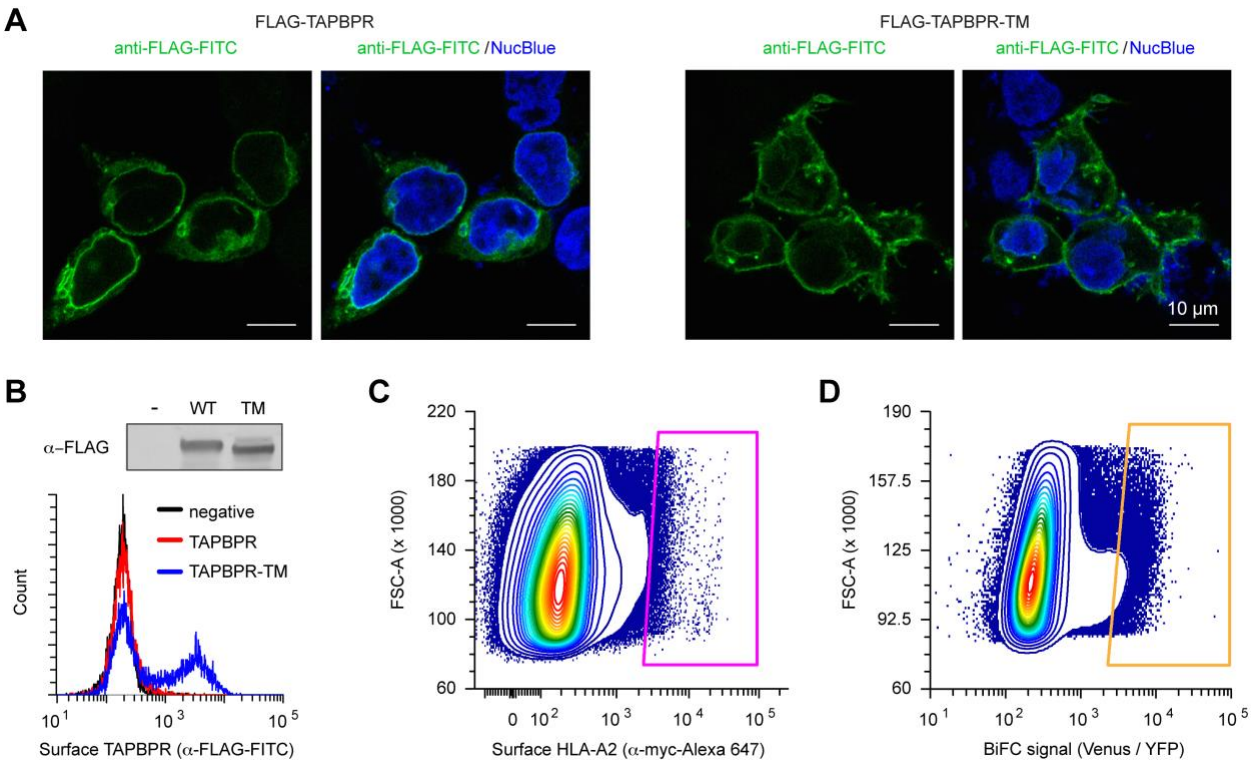

Fig. S3. Replacement of the TAPBPR transmembrane domain facilitates escape to the cell surface. (A) Confocal microscopy of HEK293 cells transfected with TAPBPR constructs that are FLAG tagged at their extracellular/luminal N-termini. Wild-type TAPBPR has intracellular localization, especially proximal to the nucleus. TAPBPR-TM localizes to the plasma membrane as well as to intracellular compartments, again especially surrounding the nucleus. **(B)** Flow cytometry analysis of surface expressed wild-type TAPBPR (red) or TAPBPR-TM (blue) in transfected Expi293F cells. Both proteins are detected by immunoblot of whole lysate (upper inset). **(C)** For selection of HLA-A*02:01 sequence variants that are surface expressed, a saturation mutagenesis library focused on the α_1/α_2 domains was constructed on HLA-A*02:01 featuring an N-terminal myc tag for surface detection and a C-terminal VN fusion for BiFC. The plasmid library was transfected in to Expi293F cells such that typically no more than a single variant is acquired by any cell. Under these conditions, most cells remain negative. Cells highly expressing surface-localized HLA-A*02:01 were collected by FACS (shown by the magenta gate, top 0.5 % of population). **(D)** For selection of HLA-A*02:01 variants competent for TAPBPR interactions, the HLA-A*02:01 library was now transfected in to Expi293F cells stably expressing TAPBPR-TM fused to VC. The top 1% of total cells for BiFC signal (orange gate) were collected, equivalent to 20 % of the Venus-positive population.

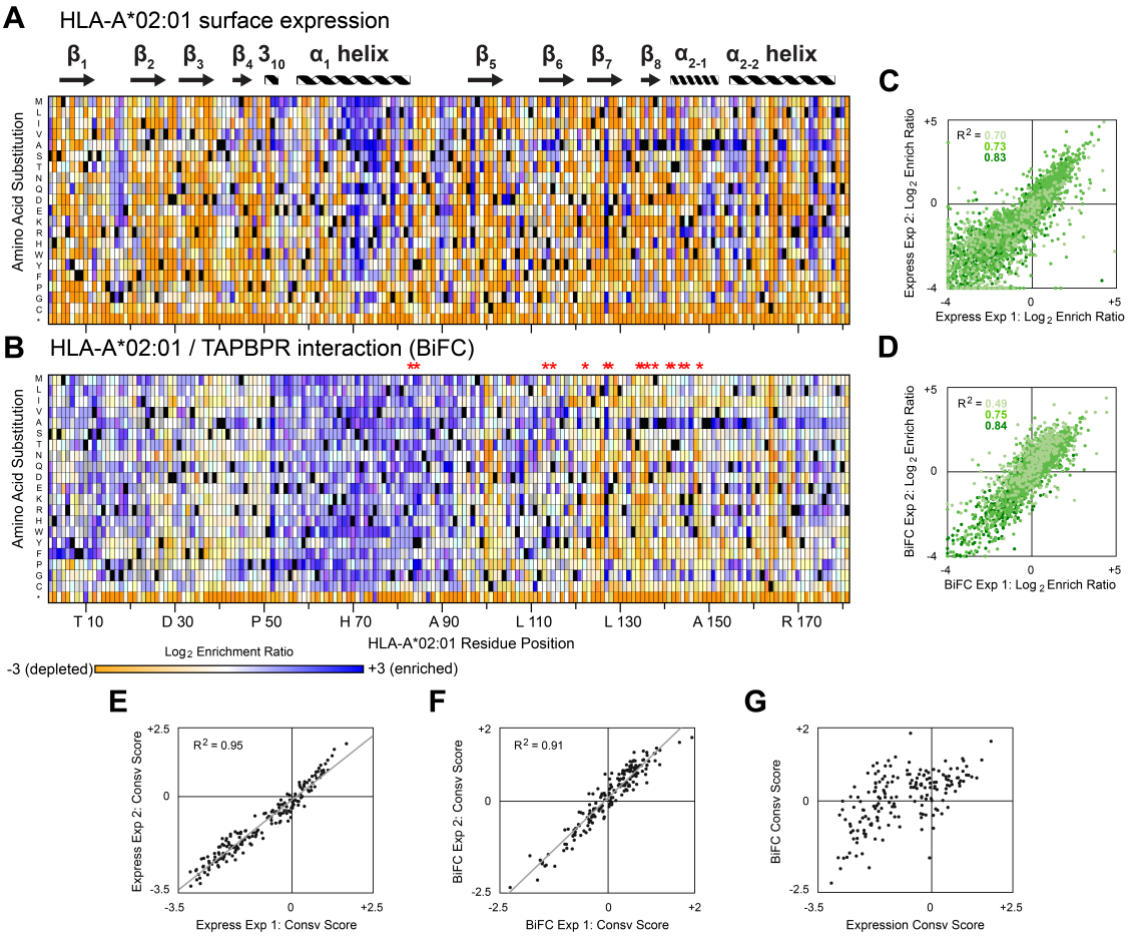

Fig. S4. Mutational landscapes of HLA-A*02:01 reveal relaxed sequence constraints for TAPBPR binding. (A) A site-saturation mutagenesis library of HLA-A*02:01 was selected by FACS for high surface expression. Residue position is on the horizontal axis, and amino acid substitutions are on the vertical axis (*, stop codon). Log_2 enrichment ratios are plotted from ≤ -3 (i.e. depleted/deleterious, orange) to ≥ +3 (enriched, dark blue). Mutations missing in the naive library (frequency ≤ 2×10^{-6}) are grey, wild-type amino acids are black. **(B)** The VN-fused HLA-A*02:01 library was selected by FACS for high BiFC in cells expressing VC-fused TAPBPR-TM. Colored as in panel B. Red asterisks (*) denote HLA-A*02:01 residues in direct contact with TAPBPR based on the homologous H2-Dd/TAPBPR X-ray structure (PDB ID 5WER). **(C and D)** Correlation plots showing the agreement of log_2 enrichment ratios for all mutations between two independent selection experiments for (C) HLA-A*02:01 surface expression or (D) HLA-A2/TAPBPR-TM BiFC. Mutations are binned from low (2×10^{-6} to 2×10^{-5}; pale green) to medium (2×10^{-5} to 2×10^{-4}; medium green) to high (≥ 2×10^{-4}; dark green) frequency in the naive library. **(E and F)** Agreement between residue conservation scores (calculated from the mean of the log_2 enrichment ratios for all non-stop mutations at a given position) from independent replicate selections for (E) HLA-A2 surface expression or (F) HLA-A*02:01/TAPBPR-TM BiFC. Conserved residues have negative scores. **(G)** Comparison of residue conservation scores between selections of the HLA-A*02:01 library for surface expression versus BiFC with TAPBPR-TM, showing that the HLA-A*02:01 sequence is more tolerant of mutations for TAPBPR interactions.

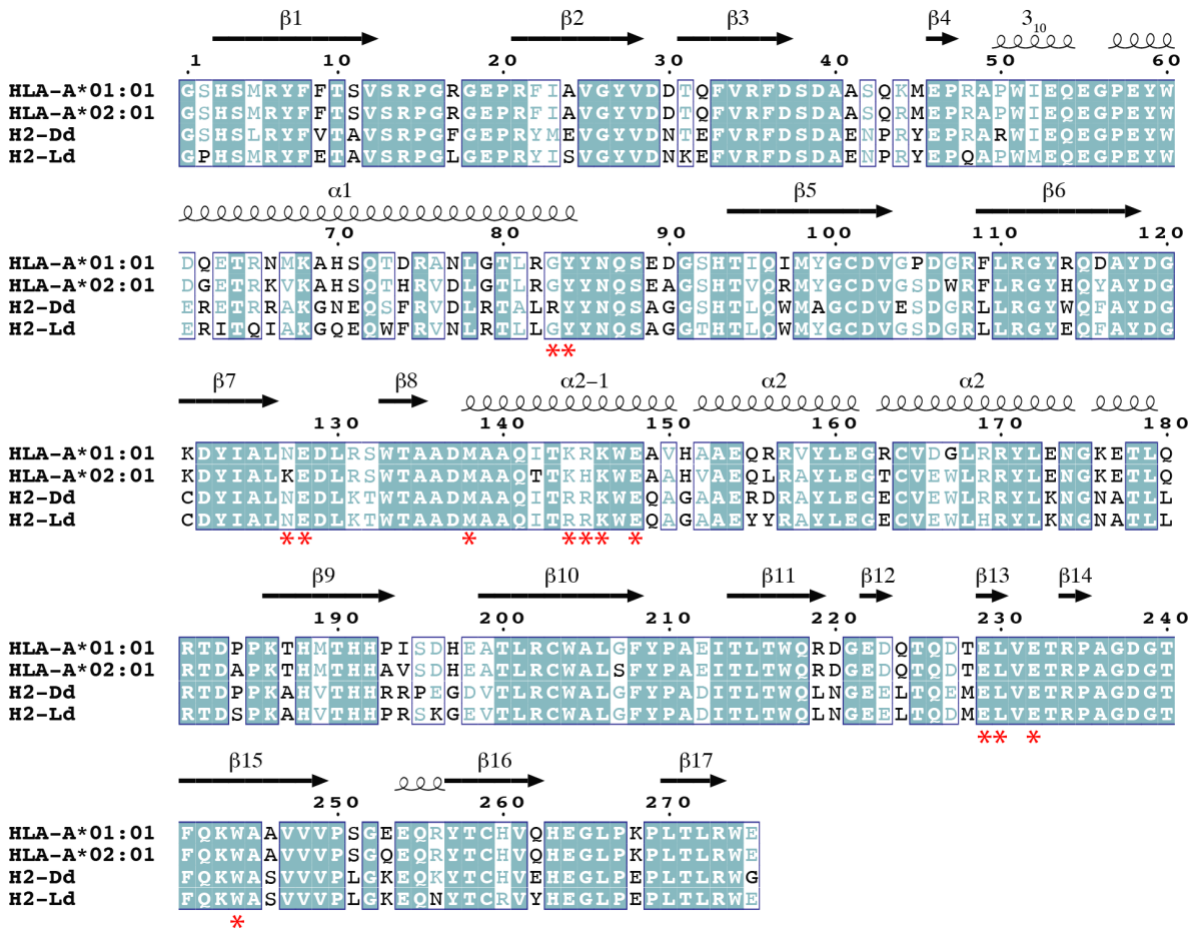

Fig. S5. **Protein sequence alignment of MHC-I molecules characterized by NMR in this study**. Sequence alignment of the luminal domains of H2-Dd (UniProtKB/Swiss-Prot: P01900), H2-Ld (UniProtKB/Swiss-Prot: P01897), HLA-A*01:01 (UniProtKB/Swiss-Prot: P30443), and HLA-A*02:01 (UniProtKB/Swiss-Prot: P01892) performed using ClustalOmega (*26*) and processed with ESPript (*27*). Secondary structure of the heavy chain from H2-Dd (PDB ID 3ECB) is provided for reference. Residues in blue boxes are conserved. The red asterisk (*) denotes heavy chain residues that are in direct contact with TAPBPR based on the structure of H2-Dd and TAPBPR (PDB 5WER) as calculated with the software Protein Interfaces, Surfaces and Assemblies (PISA) (*28*).

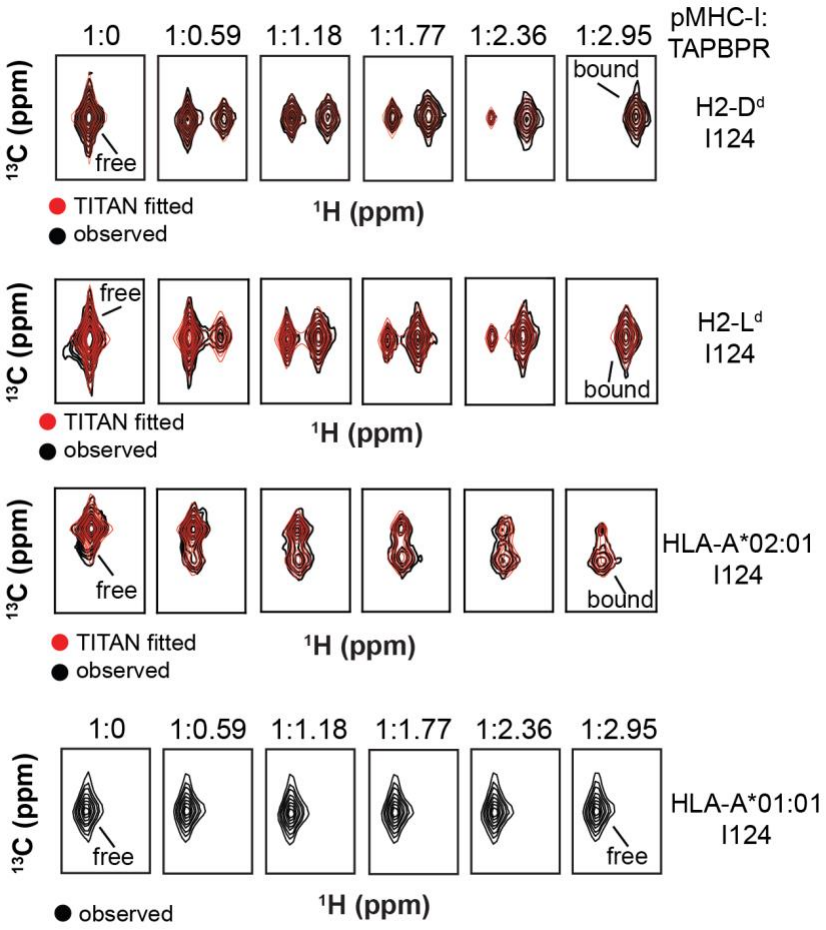

Fig. S6. **Representative titrations of pMHC-I with TAPBPR**. NMR line shape analysis, performed in TITAN (*21*), of the $^{13}C\delta1$ methyl resonance corresponding to residue I124 for H2-Dd, H2-Ld, HLA-A*02:01 and HLA-A*01:01. The experimental NMR line shapes are colored black, and the TITAN fits are colored red. Snapshots from the 2D ^{1}H-^{13}C SOFAST HMQC experiment for the NMR peak of I124 δ1 methyl are shown throughout the titration at different molar ratios of the pMHC-I to TAPBPR (further details in the Materials & Methods section). The initial concentration of the pMHC-I was 105 μM (1:0 titration point) and experiments were recorded at 25ºC at 800 MHz. The NMR peaks of the free (pMHC-I) and bound (pMHC-I/TAPBPR) states are noted. HLA-A*01:01 did not exhibit TAPBPR binding and thus was not fitted.

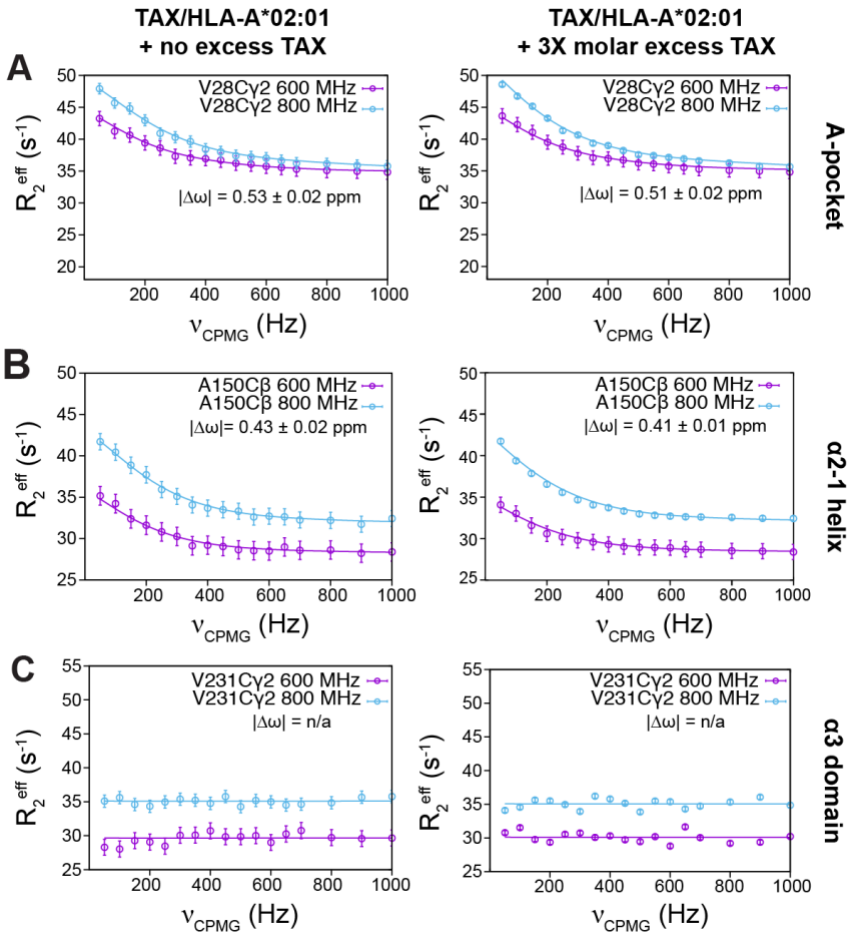

Fig. S7. Comparison of ^{13}C-SQ CPMG relaxation dispersion profiles recorded for free TAX/HLA-A*02:01/hβ2m at 1:1 and 3:1 peptide:MHC-I ratios. Profiles of ^{13}C-SQ CPMG relaxation dispersion experiments (*22*) recorded at 25°C (800 MHz – blue ; 600 MHz – purple) on AILV methyl labeled (at the heavy chain) pMHC-I. Methyl groups of each heavy chain in specified regions, including the **(A)** A-pocket, **(B)** α2-1 helix, and **(C)** α3 domain, exhibit allele-specific conformational exchange. Flat profiles indicate no observable µs-ms dynamics, compared to profiles exhibiting "curve" behavior, which are undergoing significant conformational exchange. The effective transverse relaxation rate (R_{2eff}, s^{-1}, y-axis) is shown as a function of the CPMG pulse frequency (ν_{CPMG}, Hz, x-axis). For each pMHC-I molecule the global fit of the relaxation dispersion curves performed in CATIA (http://www.biochem.ucl.ac.uk/hansen/catia/) are shown. Upper and lower error bars of R_{2eff} were determined based on the spectral noise. The fitted $|\Delta\omega|$ values are noted in each panel. CATIA fitted parameters are k_{ex} = 1102 ± 16 s^{-1} and p_B = 5.21 ± 0.02% (no excess peptide) and k_{ex} = 1126 ± 18 s^{-1} and p_B = 5.56 ± 0.02% (three-fold molar excess TAX peptide).

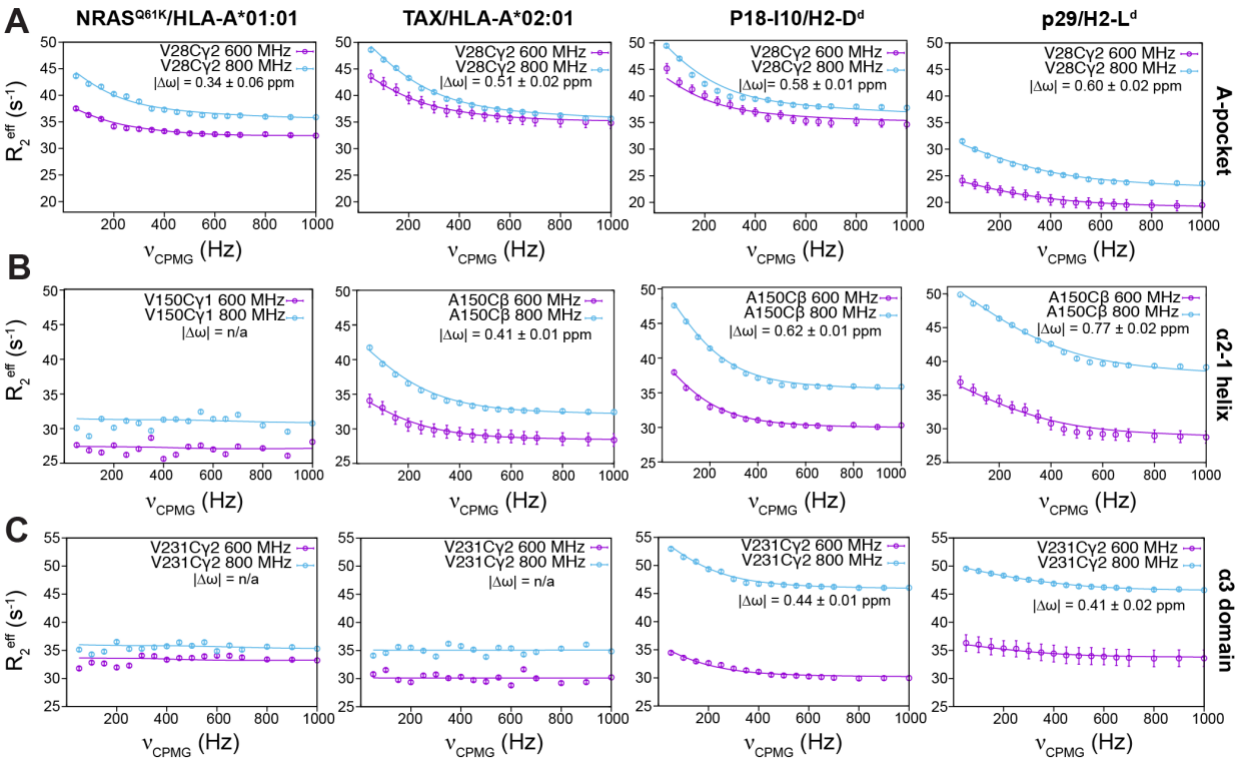

Fig. S8. Representative ^{13}C-SQ CPMG relaxation dispersion curves highlighting site-specific conformational exchange in unchaperoned pMHC-I molecules. Profiles of ^{13}C-SQ CPMG relaxation dispersion experiments (*22*) recorded at 25°C (800 MHz – blue ; 600 MHz – purple) on AILV methyl labeled (at the heavy chain) pMHC-I. Methyl groups of each heavy chain in specified regions, including the **(A)** A-pocket, **(B)** $\alpha_{2\text{-}1}$ helix, and **(C)** α_3 domain, exhibit allele-specific conformational exchange. Flat profiles indicate no observable μs-ms dynamics, compared to profiles exhibiting "curve" behavior, which are undergoing significant conformational exchange. The effective transverse relaxation rate (R_{2eff}, s^{-1}, y-axis) is shown as a function of the CPMG pulse frequency (ν_{CPMG}, Hz, x-axis). For each pMHC-I molecule the global fit of the relaxation dispersion curves performed in CATIA (http://www.biochem.ucl.ac.uk/hansen/catia/) are shown. Upper and lower error bars of R_{2eff} were determined based on the spectral noise. The fitted |Δω| values are noted in each panel and can also be found in Table S2.

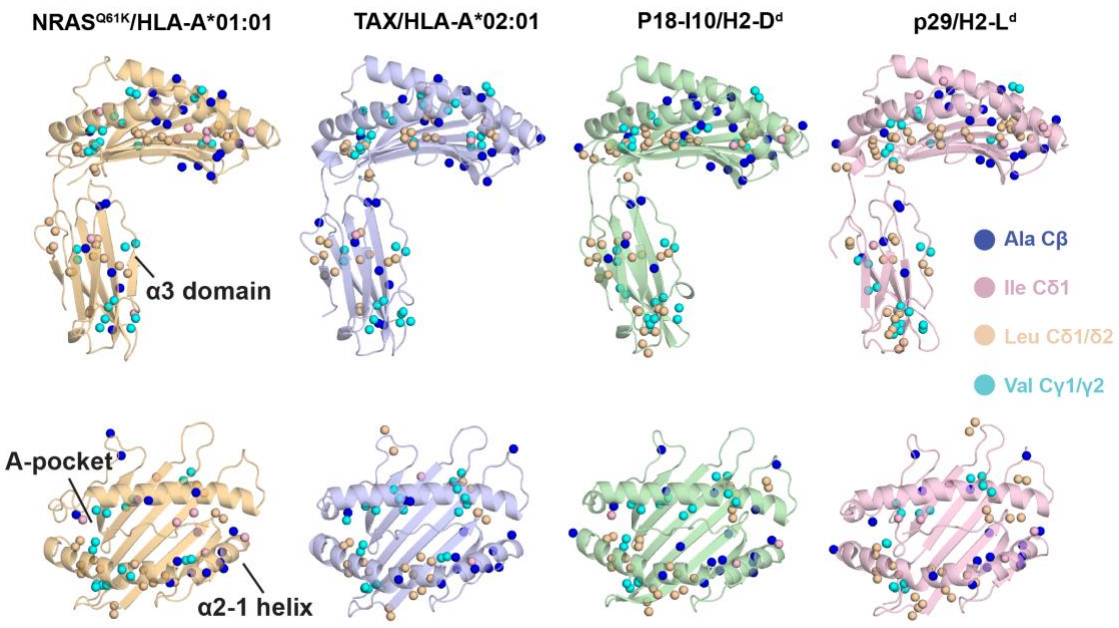

Fig. S9. Distribution of assigned AILV methyl probes on pMHC-I structures. Views of the pMHC-I molecules used in this study are shown from the side (upper images) and top of the groove (lower images). Regions of interest (A-pocket, $\alpha_{2\text{-}1}$ helix and α_3 domain) are noted. Methyl groups with assigned Ala C_β, Ile $C_{\delta 1}$, Leu $C_{\delta 1}/C_{\delta 2}$, and Val $C_{\gamma 1}/C_{\gamma 2}$ methyl resonances are shown as spheres with colors denoted in the legend on the right. The PDB IDs of the 4 alleles used are: HLA-A*01:01 (PDB ID 6MPP, light orange), HLA-A*02:01 (PDB ID 1DUZ, light blue), H2-D$_d$ (PDB ID 3ECB, light green) and H2-L$_d$ (PDB ID 1LD9, light pink).

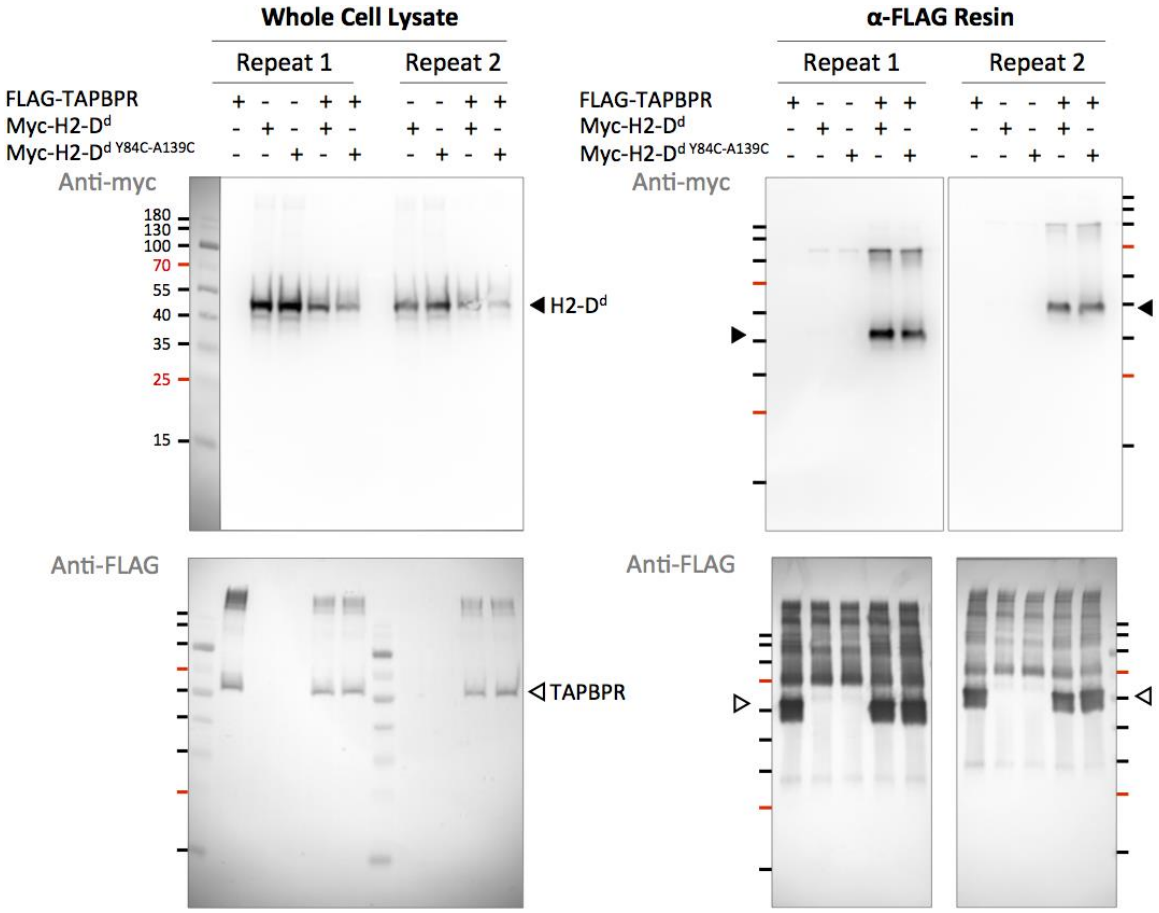

Fig. S10: Introduction of cysteines at positions 84 and 139 of H2-Dd does not prevent association with TAPBPR in cells. Human Expi293F cells were transfected with FLAG-tagged TAPBPR and/or myc-tagged H2-Dd. Total expression in cell lysate is shown by anti-myc (upper) and anti-FLAG (lower) immunoblots at left. TAPBPR complexes were immunoprecipitated with anti-FLAG resin, and after consideration of slight differences in total expression, H2-Dd and H2-Dd Y84C-A139C coprecipitate with TAPBPR at similar levels based on immunoblots at right. Sizes of molecular weight markers are indicated in kDa. Filled arrowheads indicate H2-Dd, open arrowheads indicate TAPBPR.

Supplemental Tables

pMHC-I	T_m (°C)
P18-I10/H2-D_d/hβ2m	55.0 ± 0.1
P18-I10/H2-$D_{d\ Y84C\text{-}A139C}$/hβ2m	53.0 ± 0.3
p29/H2-L_d/hβ2m	56.3 ± 0.2
TAX/HLA-A*02:01/hβ2m	63.5 ± 0.1
$NRAS_{Q61K}$/HLA-A*01:01/hβ2m	51.4 ± 0.1

Table S1. **Thermal stability of different pMHC-I molecules does not correlate with affinity for TAPBPR *in vitro***. Melting temperatures (T_m, °C) obtained from differential scanning fluorimetry experiments (*29*) are reported for each pMHC-I. Standard errors obtained from triplicate measurements are shown (n = 3). T_m values were fit using a Boltzmann sigmoidal function in GraphPad Prism v7.

Methyl Group	k_{ex} (s^{-1})	p_B (%)	|Δω| (ppm) CPMG, free pMHC-I	MHC-I
Global Fit	941 ± 17 s^{-1}	3.79 ± 0.02	-	H2-D^d
V9Cγ1 V9 Cγ2	-	-	0.477 ± 0.016 ppm 0.399 ± 0.011 ppm	H2-D^d
V12 Cγ1 V12 Cγ2	-	-	0.257 ± 0.011 ppm 0.274 ± 0.010 ppm	H2-D^d
V28 Cγ1 V28 Cγ2	-	-	0.675 ± 0.017 ppm 0.577 ± 0.013 ppm	H2-D^{dz}
A49 Cβ	-	-	0.448 ± 0.010 ppm	
L95 Cδ1 L95 Cδ2	-	-	0.373 ± 0.009 ppm 0.738 ± 0.025 ppm	H2-D^d
V103 Cγ1 V103 Cγ2	-	-	0.216 ± 0.012 ppm 0.781 ± 0.021 ppm	H2-D^d
L110 Cδ1 L110 Cδ2	-	-	0.421 ± 0.010 ppm 0.388 ± 0.009 ppm	H2-D^d
L126 Cδ1 L126 Cδ2	-	-	0.826 ± 0.021 ppm 0.718 ± 0.026 ppm	H2-D^d
A135 Cβ	-	-	0.349 ± 0.009 ppm	H2-D^d
A136 Cβ	-	-	0.341 ± 0.014 ppm	H2-D^d
A150 Cβ	-	-	0.622 ± 0.014 ppm	H2-D^d
A152 Cβ	-	-	1.247 ± 0.047 ppm	H2-D^d
A158 Cβ	-	-	0.432 ± 0.011 ppm	H2-D^d
L180 Cδ1 L180 Cδ2	-	-	0.342 ± 0.009 ppm 0.363 ± 0.009 ppm	H2-D^d
L215 Cδ1 L215 Cδ2	-	-	0.487 ± 0.011 ppm 0.411 ± 0.010 ppm	H2-D^d
L224 Cδ1 L224 Cδ2	-	-	0.273 ± 0.011 ppm 0.327 ± 0.010 ppm	H2-D^d
L230 Cδ1 L230 Cδ2	-	-	0.275 ± 0.011 ppm 0.332 ± 0.010 ppm	H2-D^d
V231 Cγ1 V231 Cγ2	-	-	0.312 ± 0.011 ppm 0.437 ± 0.010 ppm	H2-D^d
L270 Cδ1 L270 Cδ2	-	-	0.399 ± 0.009 ppm 0.392 ± 0.009 ppm	H2-D^d
Methyl Group	k_{ex} (s^{-1})	p_B (%)	|Δω| (ppm) CPMG, free pMHC-I	MHC-I
Global Fit	1700 ± 35 s^{-1}	3.21 ± 0.01 %	-	H2-L^d
V12 Cγ1 V12 Cγ2	-	-	0.335 ± 0.017 ppm 0.318 ± 0.016 ppm	H2-L^d
V28 Cγ1 V28 Cγ2	-	-	0.754 ± 0.021 ppm 0.601 ± 0.017 ppm	H2-L^d
L95 Cδ1 L95 Cδ2	-	-	0.414 ± 0.016 ppm 0.415 ± 0.015 ppm	H2-L^d
V103 Cγ1	-	-	0.318 ± 0.017 ppm	H2-L^d

V103 Cγ2			0.686 ± 0.019 ppm	
L110 Cδ1 L110 Cδ1	-	-	0.621 ± 0.016 ppm 0.565 ± 0.015 ppm	H2-L^d
L126 Cδ1 L126 Cδ2	-	-	0.722 ± 0.021 ppm 0.773 ± 0.022 ppm	H2-L^d
A135 Cβ	-	-	0.521 ± 0.015 ppm	H2-L^d
A136 Cβ	-	-	0.607 ± 0.017 ppm	H2-L^d
A150 Cβ	-	-	0.773 ± 0.022 ppm	H2-L^d
A152 Cβ	-	-	1.223 ± 0.046 ppm	H2-L^d
A158 Cβ	-	-	0.549 ± 0.016 ppm	H2-L^d
L180 Cδ1 L180 Cδ2	-	-	0.471 ± 0.014 ppm 0.462 ± 0.017 ppm	H2-L^d
L215 Cδ1 L215 Cδ2	-	-	0.627 ± 0.017 ppm 0.491 ± 0.014 ppm	H2-L^d
L224 Cδ1 L224 Cδ2	-	-	0.429 ± 0.015 ppm 0.414 ± 0.014 ppm	H2-L^d
L230 Cδ1 L230 Cδ2	-	-	0.442 ± 0.015 ppm 0.507 ± 0.015 ppm	H2-L^d
V231 Cγ1 V231 Cγ2	-	-	0.358 ± 0.017 ppm 0.409 ± 0.016 ppm	H2-L^d
L270 Cδ1 L270 Cδ2	-	-	0.440 ± 0.015 ppm 0.554 ± 0.016 ppm	H2-L^d
Methyl Group	k_{ex} (s^{-1})	p_B (%)	|Δω| (ppm) CPMG, free pMHC-I	MHC-I
Global Fit	1126 ± 18 s^{-1}	5.56 ± 0.02 %	-	HLA-A*02:01
V25 Cγ1 V25 Cγ2	-	-	0.244 ± 0.009 ppm 0.241 ± 0.009 ppm	HLA-A*02:01
V28 Cγ1 V28 Cγ2	-	-	0.513 ± 0.011 ppm 0.511 ± 0.017 ppm	HLA-A*02:01
V34 Cγ1 V34 Cγ2	-	-	0.400 ± 0.009 ppm 0.394 ± 0.009 ppm	HLA-A*02:01
A49 Cβ	-	-	0.824 ± 0.021 ppm	HLA-A*02:01
V103 Cγ1 V103 Cγ2	-	-	0.813 ± 0.020 ppm 0.821 ± 0.021 ppm	HLA-A*02:01
L110 Cδ1 L110 Cδ2	-	-	0.475 ± 0.011 ppm 0.391 ± 0.008 ppm	HLA-A*02:01
L130 Cδ1 L130 Cδ2	-	-	0.338 ± 0.008 ppm 0.413 ± 0.009 ppm	HLA-A*02:01
A149 Cβ	-	-	0.453 ± 0.009 ppm	HLA-A*02:01
A150 Cβ	-	-	0.413 ± 0.009 ppm	HLA-A*02:01
V152 Cγ1 V152 Cγ2	-	-	0.374 ± 0.008 ppm 0.351 ± 0.013 ppm	HLA-A*02:01
A153 Cβ	-	-	0.381 ± 0.009 ppm	HLA-A*02:01
L156 Cδ1	-	-	0.445 ± 0.009 ppm	HLA-A*02:01

L156 Cδ2			0.788 ± 0.025 ppm	
V165 Cγ1 V165 Cγ2	-	-	0.357 ± 0.008 ppm 0.388 ± 0.009 ppm	HLA-A*02:01
L168 Cδ1 L168 Cδ2	-	-	0.419 ± 0.009 ppm 0.418 ± 0.013 ppm	HLA-A*02:01
L172 Cδ1 L172 Cδ2	-	-	0.498 ± 0.011 ppm 0.914 ± 0.025 ppm	HLA-A*02:01
L179 Cδ1 L179 Cδ2	-	-	0.548 ± 0.010 ppm 0.589 ± 0.012 ppm	HLA-A*02:01
Methyl Group	k_{ex} (s^{-1})	p_B (%)	|Δω| (ppm) CPMG, free pMHC-I	MHC-I
Global Fit	976 ± 16 s^{-1}	5.38 ± 0.01 %	-	HLA-A*01:01
I52 Cδ1	-	-	0.454 ± 0.059 ppm	HLA-A*01:01
V28 Cγ1 V28 Cγ2	-	-	0.531 ± 0.061 ppm 0.337 ± 0.063 ppm	HLA-A*01:01
V34 Cγ1 V34 Cγ2	-	-	0.581 ± 0.064 ppm 0.447 ± 0.059 ppm	HLA-A*01:01
L179 Cδ1 L179 Cδ2	-	-	0.934 ± 0.091 ppm 1.161 ± 0.153 ppm	HLA-A*01:01

Table S2. **Summary of parameters obtained from a global fit of ^{13}C-SQ CPMG relaxation dispersion curves, performed in CATIA of different pMHC-I molecules at ^{1}H NMR fields of 600 and 800 MHz at 25°C**.

	P18-I10/H2-D$_{d\ Y84C-A139C}$/hβ2m
Data collection	
Space group	$P22_12_1$
Resolution (Å)	78.36-2.37 (2.45-2.37)
Cell dimensions	
a, b, c (Å)	66.99, 105.33, 117.27
α, β, γ (°)	90, 90, 90
R_{merge} (%)	13.8 (66.7)
Total reflections	432955 (42242)
Unique reflections	34489 (3576)
I/σ	13.2 (4.0)
$CC_{1/2}$	0.99 (0.88)
Completeness (%)	100 (100)
Redundancy	12.6 (11.8)
Refinement	
R_{work}/R_{free} (%)	18.1/25.3
Number of atoms	6482
Protein	6303
Water	179
RMS deviations	
Bond lengths (Å)	0.009
Bond angles (°)	1.26
Ramachandran Favored/Outliers (%)	100.0/0.0
B-Factor ($Å_2$)	39.2

Table S3: **X-ray crystallography data collection and refinement statistics for the P18-I10/H2-D$_{d\ Y84C-A139C}$/hβ2m complex**. Values in parentheses in the right column correspond to the highest resolution shell. PDB ID 6NPR.

REFERENCES

1. Y. Kodama, C.-D. Hu, An improved bimolecular fluorescence complementation assay with a high signal-to-noise ratio. *BioTechniques*. **49**, 793–805 (2010).

2. J. D. Heredia, J. Park, R. J. Brubaker, S. K. Szymanski, K. S. Gill, E. Procko, Mapping Interaction Sites on Human Chemokine Receptors by Deep Mutational Scanning. *J. Immunol.* **200**, 3825–3839 (2018).

3. E. Procko, R. Hedman, K. Hamilton, J. Seetharaman, S. J. Fleishman, M. Su, J. Aramini, G. Kornhaber, J. F. Hunt, L. Tong, G. T. Montelione, D. Baker, Computational design of a protein-based enzyme inhibitor. *J. Mol. Biol.* **425**, 3563–3575 (2013).

4. J. Park, B. Selvam, K. Sanematsu, N. Shigemura, D. Shukla, E. Procko, Structural architecture of a dimeric class C GPCR based on co-trafficking of sweet taste receptor subunits. *J. Biol. Chem.* **294**, 4759–4774 (2019).

5. D. M. Fowler, C. L. Araya, W. Gerard, S. Fields, Enrich: software for analysis of protein function by enrichment and depletion of variants. *Bioinformatics*. **27**, 3430–3431 (2011).

6. A. C. McShan, K. Natarajan, V. K. Kumirov, D. Flores-Solis, J. Jiang, M. Badstübner, J. S. Toor, C. R. Bagshaw, E. L. Kovrigin, D. H. Margulies, N. G. Sgourakis, Peptide exchange on MHC-I by TAPBPR is driven by a negative allostery release cycle. *Nat. Chem. Biol.* (2018), doi:10.1038/s41589-018-0096-2.

7. G. K. Balendiran, J. C. Solheim, A. C. Young, T. H. Hansen, S. G. Nathenson, J. C. Sacchettini, The three-dimensional structure of an H-2Ld-peptide complex explains the unique interaction of Ld with beta-2 microglobulin and peptide. *Proc. Natl. Acad. Sci. U.S.A.* **94**, 6880–6885 (1997).

8. R. Wang, K. Natarajan, D. H. Margulies, Structural basis of the CD8αβ/MHCI interaction: focused recognition orients CD8β to a T cell proximal position. *J Immunol*. **183**, 2554–2564 (2009).

9. J. S. Toor, A. A. Rao, A. C. McShan, M. Yarmarkovich, S. Nerli, K. Yamaguchi, A. A. Madejska, S. Nguyen, S. Tripathi, J. M. Maris, S. R. Salama, D. Haussler, N. G. Sgourakis, A Recurrent Mutation in Anaplastic Lymphoma Kinase with Distinct Neoepitope Conformations. *Front Immunol*. **9**, 99 (2018).

10. A. R. Khan, B. M. Baker, P. Ghosh, W. E. Biddison, D. C. Wiley, The structure and stability of an HLA-A*0201/octameric tax peptide complex with an empty conserved peptide-N-terminal binding site. *J. Immunol.* **164**, 6398–6405 (2000).

11. G. I. Morozov, H. Zhao, M. G. Mage, L. F. Boyd, J. Jiang, M. A. Dolan, R. Venna, M. A. Norcross, C. P. McMurtrey, W. Hildebrand, P. Schuck, K. Natarajan, D. H. Margulies, Interaction of TAPBPR, a tapasin homolog, with MHC-I molecules promotes peptide editing. *Proc. Natl. Acad. Sci. U.S.A.* **113**, E1006-1015 (2016).

12. M. D. Winn, C. C. Ballard, K. D. Cowtan, E. J. Dodson, P. Emsley, P. R. Evans, R. M. Keegan, E. B. Krissinel, A. G. W. Leslie, A. McCoy, S. J. McNicholas, G. N. Murshudov, N. S. Pannu, E. A. Potterton, H. R. Powell, R. J. Read, A. Vagin, K. S. Wilson, Overview of the CCP4 suite and current developments. *Acta Crystallogr D Biol Crystallogr*. **67**, 235–242 (2011).

13. A. J. McCoy, R. W. Grosse-Kunstleve, P. D. Adams, M. D. Winn, L. C. Storoni, R. J. Read, Phaser crystallographic software. *J Appl Crystallogr*. **40**, 658–674 (2007).

14. P. Emsley, K. Cowtan, Coot: model-building tools for molecular graphics. *Acta Crystallogr. D Biol. Crystallogr.* **60**, 2126–2132 (2004).

15. P. D. Adams, P. V. Afonine, G. Bunkóczi, V. B. Chen, I. W. Davis, N. Echols, J. J. Headd, L.-W. Hung, G. J. Kapral, R. W. Grosse-Kunstleve, A. J. McCoy, N. W. Moriarty, R. Oeffner, R. J. Read, D. C. Richardson, J. S. Richardson, T. C. Terwilliger, P. H. Zwart, PHENIX: a comprehensive Python-based system for macromolecular structure solution. *Acta Crystallographica Section D Structural Biology*. **D66**, 213–221 (2010).

16. K. Natarajan, A. C. McShan, J. Jiang, V. K. Kumirov, R. Wang, H. Zhao, P. Schuck, M. E. Tilahun, L. F. Boyd, J. Ying, A. Bax, D. H. Margulies, N. G. Sgourakis, An allosteric site in the T-cell receptor Cβ domain plays a critical signalling role. *Nature Communications*. **8**, 15260 (2017).

17. P. Rossi, Y. Xia, N. Khanra, G. Veglia, C. G. Kalodimos, 15N and 13C- SOFAST-HMQC editing enhances 3D-NOESY sensitivity in highly deuterated, selectively [1H,13C]-labeled proteins. *J Biomol NMR*. **66**, 259–271 (2016).

18. V. Tugarinov, L. E. Kay, Ile, Leu, and Val methyl assignments of the 723-residue malate synthase G using a new labeling strategy and novel NMR methods. *J. Am. Chem. Soc.* **125**, 13868–13878 (2003).

19. F. Delaglio, S. Grzesiek, G. W. Vuister, G. Zhu, J. Pfeifer, A. Bax, NMRPipe: a multidimensional spectral processing system based on UNIX pipes. *J. Biomol. NMR.* **6**, 277–293 (1995).

20. W. Lee, M. Tonelli, J. L. Markley, NMRFAM-SPARKY: enhanced software for biomolecular NMR spectroscopy. *Bioinformatics*. **31**, 1325–1327 (2015).

21. C. A. Waudby, A. Ramos, L. D. Cabrita, J. Christodoulou, Two-Dimensional NMR Lineshape Analysis. *Sci Rep*. **6** (2016), doi:10.1038/srep24826.

22. P. Lundström, P. Vallurupalli, T. L. Religa, F. W. Dahlquist, L. E. Kay, A single-quantum methyl 13C-relaxation dispersion experiment with improved sensitivity. *J. Biomol. NMR.* **38**, 79–88 (2007).

23. J. Jiang, K. Natarajan, L. F. Boyd, G. I. Morozov, M. G. Mage, D. H. Margulies, Crystal structure of a TAPBPR–MHC-I complex reveals the mechanism of peptide editing in antigen presentation. *Science*, eaao5154 (2017).

24. Y. Song, F. DiMaio, R. Y.-R. Wang, D. Kim, C. Miles, T. Brunette, J. Thompson, D. Baker, High-Resolution Comparative Modeling with RosettaCM. *Structure*. **21**, 1735–1742 (2013).

25. P. Conway, M. D. Tyka, F. DiMaio, D. E. Konerding, D. Baker, Relaxation of backbone bond geometry improves protein energy landscape modeling. *Protein Sci.* **23**, 47–55 (2014).

26. F. Sievers, A. Wilm, D. Dineen, T. J. Gibson, K. Karplus, W. Li, R. Lopez, H. McWilliam, M. Remmert, J. Söding, J. D. Thompson, D. G. Higgins, Fast, scalable generation of high-quality protein multiple sequence alignments using Clustal Omega. *Mol Syst Biol*. **7**, 539 (2011).

27. X. Robert, P. Gouet, Deciphering key features in protein structures with the new ENDscript server. *Nucleic Acids Res*. **42**, W320–W324 (2014).

28. E. Krissinel, K. Henrick, Inference of macromolecular assemblies from crystalline state. *J. Mol. Biol.* **372**, 774–797 (2007).

29. L. M. Hellman, L. Yin, Y. Wang, S. J. Blevins, T. P. Riley, O. S. Belden, T. T. Spear, M. I. Nishimura, L. J. Stern, B. M. Baker, Differential scanning fluorimetry based assessments of the thermal and kinetic stability of peptide-MHC complexes. *J. Immunol. Methods*. **432**, 95–101 (2016).